

## **Physical properties, morphology and petrological characteristics of pumices from the Central Indian Ocean Basin**

Niyati G. Kalangutkar\*, Sridhar D. Iyer and D. Ilangovan  
National Institute of Oceanography (Council of Scientific and Industrial Research),  
Dona Paula, Goa 403 004, India.

\* Corresponding author. Tel.: +91 832 2450 244; Fax: +91 832 2450 609

E-mail addresses: niyati.kalangutkar@gmail.com.

### **Abstract**

About 400 pumice clasts collected from the Central Indian Ocean Basin (CIOB) were studied for their morphology and were classified based on their shape and size. A majority of the samples range between <1 cm and 36 cm and in the Zingg's shape diagram plot in the equant and oblate fields. The Corey Shape Factor for most of the samples is close to 0.7, which is common for volcanoclastic material. The physical properties such as density, specific gravity, void ratio, porosity, moisture content and degree of saturation, were determined for thirty pumice samples. Density varies from 0.21 to 0.74 gm/cc, specific gravity 1.84 to 2.75, void ratio 2 to 10, porosity 67% to 91%, moisture content during sinking 0.44 to 2.35 and degree of saturation varies from 0.44 to 1.89. Binocular and electron microscopy studies reveal that 60% of the vesicles are elongated, 30% are spherical and 10% are fibrous. Petrography of the pumices exhibits vitrophyric texture with phenocrysts of feldspars and clinopyroxenes. X-ray diffractogram and mineral analyses confirm plagioclase to be a major phase while quartz and orthoclase are not uncommon. Todorokite is commonly present in the ferromanganese oxide coating present over some of the pumices. The paper also delves into some details concerning the controversial origin of the pumices and glass shards in the CIOB.

**Keywords:** pumice, physical properties, submarine.

## **1. Introduction**

Pumice, a characteristic product of convergent zone volcanism has been reported to occur from several places surrounding the major oceans but rarely at abyssal depths. The low density of the pumices enables their transportation to long distances by water or air. The study of drifted pumice would lead to important conclusions on the source, the tectonics and geochemical regime of the area, volatiles and vapor pressures prevailing during the emplacement of the magma (Bryan, 1971). Furthermore, sea-rafted pumice can provide a record of submarine silicic explosive volcanism that may not be otherwise recorded.

Pumice and ash particles from submarine pyroclastic flow deposits are more intriguing than their subaerial counterparts. Pumice is easily abraded during transport by particle-to-particle contact and thus differences in the extent of particle interactions during various modes of transport could result in distinctive morphological characteristics. The morphologic complexity for the submarine samples is likely a result of secondary fracturing of pumice clasts, which is attributed to thermal shock and phreatic explosions (Morelli and Carey, 2004). The importance of investigating the morphology and texture of pumice clasts cannot be under estimated as these provide information concerning the behaviour of a silicic magma in terms of its vesiculation, fragmentation and ascent (e.g., Klug et al., 2002; Polacci et al., 2003).

Iyer and Sudhakar (1993) reported the existence of a large pumice field in the Central Indian Ocean Basin (CIOB). The CIOB hosts a pumice field that covers an area of 600,000 sq km which is about 1/9<sup>th</sup> of the basinal area. In view of the above, the objectives of this paper were to study the physical, morphological and petrological characteristics of pumices recovered from the basin. Furthermore, the controversy concerning the source of these pumices is expounded.

## **2. Regional settings and sampling**

The CIOB has been extensively explored under India's national project, "Surveys for Polymetallic Nodules". The area under investigation extends from 9° to 16° S latitude and 72° E to 80° E longitude and has an average water depth of 5100 m. Several investigators have reported on the different geological aspects of this basin, such as sedimentological characteristics (types, minerals, geochemistry), bathymetry and morphotectonic features (fracture zones, seamounts, hills, lineaments), ferromanganese deposits (nodules, crusts), occurrence of a variety of volcanics, probable hydrothermal events and the relation between volcanics and the ferromanganese deposits (Kodagali, 1998; Iyer 2005; Mukhopadhyay, et al., 2002; Das et al., 2007; Kalangutkar et al. 2007).

The ferromanganese samples (nodules, encrustations and crusts) were collected using free-fall grabs, Petterson grabs and dredges and in most instances pumice clasts were also recovered with these samples. It was noted that pumice clasts are abundant near morphotectonic features like fracture zones and seamounts (Fig. 1).

### **3. Materials and Methods**

A little more than 400 pumice samples from the CIOB (Fig. 1) were studied for their morphological parameters. Using a vernier caliper, the length (a), breadth (b) and thickness (c) were measured and their ratios were plotted in a Zingg's diagram. Zingg's (1935) used the ratios  $b/a$  and  $c/b$  of sediment grains to define four shape classes: oblate, prolate, bladed and equant. Wilson and Huang (1979) opined that for aerial pyroclastic fallout, neither the Zingg's classification nor the Corey shape factor (CSF) were found to be good expressions of particle shape, due mainly to the fact that the irregular volcanic particles tumble as they fall in air. Although this could be a constraining factor but the Zingg's classification was successfully used by Iyer and Karisiddaiah (1988) to identify the shape of 48 pumice samples from the CIOB. Here we have used the same classification to categorize the major shapes of the pumice clasts and the data have been used for various plots (Figs. 2 and 3).

The selected samples were made free from seawater salt and later used for making thin sections and powders for X-ray Diffraction (XRD) studies. Chips of salt-free samples were mounted on stubs and observed under a Scanning Electron Microscope (SEM) and Energy Dispersive Spectroscopy (EDS). The SEM system used was a JSM 5800 LV, JEOL fitted with EDS of INCA make. The operational conditions during the SEM study were 20 mm working distance and 20 kV voltage and for EDS a 10 mm working distance and 20 kV voltage were used.

The pumices were powdered using a Retsch PM 400-ball mill. X-ray analysis was carried out, using a Philips XRD (PW 1840 model) with Cu  $K\alpha$  as target, between  $8^\circ$  and  $45^\circ$   $2\theta$  at a speed of  $0.02^\circ$   $2\theta/\text{sec}$  (or  $1.2^\circ$   $2\theta/\text{min}$ ) while the chart speed was 10 mm/  $2\theta$ . The ferromanganese (FeMn) oxide coated samples were hand ground using mortar and pestle and were scanned between  $8^\circ$  and  $40^\circ$   $2\theta$  at  $0.02^\circ$   $2\theta/\text{sec}$  (or  $1.2^\circ$   $2\theta/\text{min}$ ) scan speed.

Forty samples were cleaned in an ultra sonic cleaner, dried and were viewed under a binocular microscope for their morphological features. Thirty pumice samples were cut into cubes of approximately 1 cubic centimeter, weighed and placed in beakers containing seawater. The samples initially floated due to their low density and thereafter got water saturated. The new weight of the

sample was recorded after every 5, 10, 15 and 20 minutes till the samples got water logged and sank to the bottom of the beaker. The thirty samples were powdered, weighed and used for the determination of specific gravity. Based on these results other parameters like void ratio, porosity, water content during sinking, saturation density and porosity were calculated (Table 1).

#### **4. Results and Interpretations**

##### **4.1 Morphological studies**

Morphologically, the CIOB pumices exhibit a variety of shapes such as irregular, oval, sub-rounded and rounded (Fig. 4) and are gray, white and buff in colour. The size ranges from 0.5 mm to 150 mm in length while a 360 mm long specimen has also been recovered. Based on a study of 3083 pumices from 10,000 locations, Sudhakar et al. (1992) reported that size-wise 94% of the population are

< 4 cm and 1% represent >8 cm, and that 84% were non-coated with FeMn oxides and 16% were either coated or occurred as nuclei and substrate for the FeMn oxides.

Based on the presence or absence of FeMn oxides we grouped the pumices into two categories:

(1) Coated with FeMn oxides: In this category we have noted that 25% of the pumices occur either within the nodules that have upto 5 mm oxide thickness or else the pumices have a thin veneer or spots of FeMn oxides (Fig. 4). The coated pumices show features of attrition and have a dull colour due to the presence of FeMn oxides.

(2) Uncoated or fresh pumices: these types of pumices are generally whitish or buff in color, rounded to oval shaped and form ~75% of the total studied samples.

Considering the morphological measurements, a discriminatory plot was made to identify the Zingg's shape class of the 400 pumice clasts (Fig. 2a). It is observed that most of the samples fall in oblate (32%) and equant (30.7%) fields whilst a few samples are prolate (21% i.e., rod shaped) and flattened disc shaped (16.3%). Similarly, of the 48 samples studied by Iyer and Karisiddaiah (1988) 33% were equant and ~17% were oblate.

To understand the role of the axes (a, b, c) in controlling the shape and settling of the 400 pumice clasts, several plots were made. Significant correlation exists between the axes (a, b, and c)

while the ratio of two axes is seen to be variable. The linear positive trends suggest the three axes to vary proportionately and this indicates a good correlation with the Zingg's ratio plot wherein most of the samples fall in the field of oblate and equant shape.

The shape of the 400 pumices was determined by two methods: sphericity ( $[(c^2/ab)^{1/3}]$ ) and also by the CSF calculation ( $c/[ab]^{1/2}$ ). These parameters help to evaluate the degree of departure of a grain or clast from a sphere that typically has an average value of 1. It is noted that the greater the departure from the spherical nature the smaller is the value of CSF and this causes a decrease in its settling velocity within a fluid (Komar and Reimers, 1978). The studied samples were plotted on a histogram (Fig. 2b), which depicts that a majority of the samples have CSF values less than that for naturally occurring clastic material. It is observed that 66 samples (~17%) fall within the range of 0.4 to 0.5, 85 samples (22%) within 0.5-0.6, 56 samples (14%) within 0.6-0.7, 48 samples (12%) within 0.7-0.8 and 34 samples (9%) within 0.9-1. The CSF ranges between 0.046 and 0.935 (avg 0.49) for the studied samples while Iyer and Karsiddhaiah (1988) obtained a range between 0.17 and 0.77 for a limited number of samples. The average CSF of their samples is 0.47, which is close to the present study yet these averages are less than that for naturally occurring clastic material (0.7) (Jimenez and Madsen, 2003).

It was noted that on the plots of CSF vs a, b and c axes and sphericity vs a, b and c axes the values of correlation coefficients for CSF and sphericity are similar. Most of the sphericity values range from 0.4 to 1. The plots indicated that the length ('a') and breadth ('b') have a lesser influence on the sphericity in comparison to the height or thickness ('c') of the samples.

Several plots of the ratios (c/b, c/a and b/a) against CSF values (Fig. 3) were considered to understand the controlling parameter on the shape of the CIOB pumice. The linear positive trends suggest the ratios c/b and c/a to vary proportionately with CSF values (Fig. 3 a, b) indicating that these have a control on the CSF. At a value greater than 0.8 CSF i.e., as the sample nears a spherical shape, there is less variation in the c/a ratio as indicated by the curved nature of the plot (Fig. 3 b). The plot of b/a with CSF values (Fig. 3 c) shows the latter to range between 0.4 and 1 and no linear correlation is noted. Therefore, the ratios c/b and c/a apparently control the sphericity of the samples. Similar results were observed in plots of c/b, c/a and b/a, against the sphericity which again attest to the important role played by the c-axis.

## 4.2 Sinking experiment

Physical properties of thirty pumice samples were used for the sinking experiment and the degree of saturation required for sinking of all the pumices was calculated. The relation between time and density during sinking is shown (Fig. 5) which indicates that with increasing time, the pumice density increases due to saturation and eventually sinks. A majority of the samples took two days to reach a point of saturation and sink while two samples took 43 and 56 days to sink. Hence, the rate of sinking not only depends upon the density and permeability of the samples but also on the nature of the vesicles. It is recognised that although in due course of time even low-density pumice would sink, because generally all the pores in a specimen would be interconnected, but sinking would depend on the size of the specimen. Whitham and Sparks (1986) have shown that the largest samples absorb proportionally less water than smaller samples and would remain afloat for a longer time. Experiments by Manville et al. (1998) supported this contention that the time required for a pumice clast to saturate is proportional to the square of its radius, i.e

$$t \propto r^2.$$

Esposito and Guadagno (1998) investigated pumices belonging to the 79 AD Mount Vesuvius eruption and found that although the particles sink when their density exceeds but it takes longer time to achieve apparent saturation (constant weight) of the particles. For instance, the 16 mm sized particles sank in about 3 days but it took about 5 days for the occurrence of apparent saturation. Furthermore, pumices from Astroni (Phlegraean vent field, Italy), that were between 4 and 8 mm in size required about a week to sink, while the apparent saturation of the larger clasts took more than two months. The authors believe that the differential sinking rates could be due to the presence of inter- and intra-particles voids within the pumices.

From a study of a 1962 submarine eruption in the South Sandwich Islands, Risso et al. (2002) observed that most samples (rarely smaller than 5 cm or larger than 30 cm) were from low-density, highly vesiculated (spherical to ellipsoid vesicles) pumice, and they behave in a similar manner way. Those authors found that the curve (water absorption vs density) could be segmented into three parts with successive low, high and again low gradient. One sample deviated from this observation and it was found that this sample was a small, dense pumice clast with thin elongated (tubular) vesicles. It absorbed water very slowly and could remain afloat longer than the other smaller or larger fragments used for the experiments. Interestingly, similar plots for the CIOB pumices (Fig. 5) did not reveal

such segmentations which could indicate that all the samples showed almost a constant linear absorption rates and this could be due to nature of the vesicles of these pumices.

### **4.3 Physical properties**

The data for dry density, specific gravity, porosity, void ratio and moisture content and saturation density at the time of sinking for the thirty pumices from the CIOB are tabulated in (Table 1). It can be seen that the dry density of the samples varies from 0.21 to 0.74 gm/cc (avg. 0.43 gm/cc) and the specific gravity ranges between 1.84 and 2.75 (avg. 2.34) these results correspond to rhyolite-andesite. The glass shards and CIOB pumices have an andesitic to rhyolitic composition (Martin-Barajas and Lallier-Verges, 1993; Iyer and Sudhakar 1993; Iyer et al., 1997; Pattan et al., 1999; Iyer, 2005) similar to the pyroclasts from Krakatau eruptions (Nishimura et al., 1992). The higher values of specific gravity in some samples could be due to the presence of FeMn oxides trapped within the vesicles. A maximum porosity (91.43%) and maximum void ratio (10.67) is shown by a clast with the least density (0.21 gm/cc), whereas the minimum porosity (67%) and minimum void ratio (2.03) is exhibited by a clast that has a highest dry density (0.74 gm/cc; Table 1). Hence, it is observed that porosity and density are negatively correlated. Since denser samples require a lesser degree of saturation to sink, therefore, samples with higher porosity require a higher degree of saturation to get water logged and sink because as porosity increases density decreases. In reality this might not be the case because connected vesicles or the permeability of the vesicles may play an important role in determining the sinking rate of the pumice.

### **4.4 Binocular studies**

Several supporting studies were undertaken to characterise the CIOB pumices. Binocular microscopy reveals fibrous fragments with tabular and elongated vesicles in most of the samples. At places the glassy filaments show features of swirling and twisting (Fig. 6 a). The smaller vesicles are mostly spherical while coalesced vesicles have resulted in larger oval shaped ones. Pumice clasts with non-fibrous vesicles are less abundant. In general, the size of the vesicles varies from 50 to 150  $\mu\text{m}$ . Spherical glass bubbles giving rise to triple junction bubble walls are also observed while elongated bubbles are more abundant near mafic minerals (Fig. 6 b). Some of these bubbles are broken and are seen in smooth textured pumices (Fig. 6 d). The larger vesicles are seen to contain minerals (Fig. 6 c), radiolarians and manganese micronodules. While crystals of quartz are distinct it is probable that the other minerals may be those of feldspar, biotite and magnetite.

## **4.5 Petrography**

Thin section studies of pumice reveal phenocrysts of plagioclase, biotite, clinopyroxene and ore minerals in a glassy and vesicular groundmass. Plagioclase phenocrysts and microlites are lath shaped and show lamellar twinning. Zoning is distinct in one of the plagioclase grains (Fig. 6 e). At places glomeroporphyritic texture is exhibited by laths of plagioclase and pyroxenes (Fig. 6 f). Biotite grains are rarely present and show pleochroism in shades of brown. The glassy groundmass shows isolated, non-connected, oval shaped vesicles in some samples while a few others are highly fibrous, have well-connected vesicles and exhibit a swirled texture. The vesicular shapes (spherical, oval, elongated) and sizes (20-400  $\mu\text{m}$ ) show intra- and inter-clast variations.

## **4.6 XRD studies**

The XRD profiles indicated the pumices to be highly silicic and glassy as evident from the hump between  $20^\circ$  and  $30^\circ$  (Fig.7). Quartz and plagioclase occur as the major mineral phases while augite and fayalite are less common. Cristobalite quartz is also identified as one of the phases (Fig.7). Pumice vesicles were seen to contain drusy crystals, which could be of cristobalite as it can form even by vapour phase crystallisation. Plagioclase is represented by labradorite and some amount of anorthoclase. X-ray analysis of the FeMn oxides reveals the presence of todorokite, manganite, maghemite and hematite. These results support the earlier observations (Iyer and Karisiddaiah, 1988).

## **4.7 Scanning Electron Microscopy studies**

Under the SEM most of the pumice samples show irregular to elongated vesicles with sizes ranging from 10 to 400  $\mu\text{m}$ . Pumices with irregular vesicles show a number of euhedral crystals occupying the vesicles. The samples with highly elongated fibrous or filamentous vesicles (Fig. 8 a, b) and with spherical interconnected vesicles (Fig. 8 c, d) do not show the presence of any crystals. Bubble wall triple junction is exhibited in several samples that have spherical vesicles (Fig. 8 d). Change in vesicle nature from elongated to fibrous is seen within a clast (Fig. 8 e). Some of the crystals have a coating of glass (Fig. 8 f). Radiolarians are seen to be trapped within some of the vesicles (Fig. 8 g). EDS of a few minerals show these to be plagioclase (andesinic to labradoritic) with An content of 35-55, while a high value of An 70 is observed in one sample. The SEM of FeMn oxides showed botryoidal structures made up of todorokite (Fig. 8 h).



## 5. Discussions

Pumices resulting from silicic eruptions would not only exhibit differences in their gross macroscopic features but may also have discrete microscopic traits as reflected by their vesicularities (shape, size, distributions, vesicle wall thickness, interconnectivity; Polacci et al., 2003). The range of morphology and textural characteristics of the pyroclasts, ensuing either during different or even within the same eruption phase, may be either related to variations in eruption dynamics (Gardner et al., 1996; Klug et al., 2002) or development of heterogeneous flow conditions in the conduit (Polacci et al., 2001).

As seen from the Zingg ratio (Fig. 2a) the shapes of the CIOB pumices are variable: 32% oblate, 31% are equant, 21% prolate and 21% bladdled. Given that the morphology of the clasts affects the settling velocities, the equant clasts can remain in suspension for a longer time as compared to the non-equant clasts since its settling velocities are close to that of a sphere. This in turn probably indicates the source of the pumice clasts (e.g., Goldbery and Richardson, 1989) because the non-equant clasts, of oblate or prolate shape (Fig. 2a), must have settled more rapidly. Pumice with long and inter-connected vesicles is more easily water-logged and hence sinks rapidly, whilst rounded and non-connected vesicles keep them afloat for a longer time (Binns, 1972). Hence, it is assumed that the more spherical clasts have settling velocities similar to that of a sphere and therefore remains afloat for a longer time and could drift to distant places. This observation has a bearing on the source of the pumices in that the clasts with lower settling velocities may be derived from a source nearer to the site of deposition, which could be within or near the CIOB.

The experiments by Whitham and Sparks (1986) support the theory that hot pumice sinks immediately on immersion in water despite having a lower density than water. In contrast, colder pumice tends to float and hence could drift for kilometres across the ocean waters but with time the cold pumices get water logged and eventually sink. The time taken for enough water to be absorbed to sink depends on pumice size, initial density, size distribution of vesicles and the connectedness of the vesicles. SEM studies of vesicle microstructure indicate that connections between vesicles occur by bubble coalescence and cracking of vesicles (Mangan and Cashman, 1996). In the case of the unconnected pore space it is assumed that closed-off vesicles are distributed in the same way as connected ones and forms a continuous medium (Manville et al., 1998).

Our observation from the sinking experiments conducted on CIOB pumices indicate that density, vesicle shape, porosity and connectedness of the vesicles are all interrelated and no single

factor determines the settling rates for the pumices. A single clast, having different parametric values depending on the nature and type of vesicles, probably suggests the rapidly changing characteristics of the pumice eruptions. Equant shape and high CSF settling values are indicated by a positive correlation ( $r=0.89$ ) between  $c/b$  and CSF and the closeness of the settling velocities to that of a sphere. The habitation by organisms within the vesicles may influence the settling of pumice (Fig. 8 g) (Iyer and Karisiddaiah, 1988).

The experiments of Zhang (1998) on the behavior of viscous liquid suggest that the bubbles formed are initially roughly spherical, and then become oblate with the short axis oriented vertically and finally to tear-drop shaped. These changes in the shape of the bubble occur due to the ascension of the magma under lowered hydrostatic pressure. As seen from binocular microscopy studies, elongated bubbles are more abundant in the vicinity of crystals (Fig. 6 b). Similar observations were carried out on pumice pyroclasts from the Chaos Crags, California (Heiken and Eichelberger, 1980) and those authors suggested that pockets of large vesicles surrounding phenocrysts could grow in a few seconds and that the vesicles could have begun development several kilometres below the ground surface. According to Sparks (1978) it is possible for vesicle growth to begin at a depth of 2 or 3 km in rhyodacitic melts that have a water content of 3% or more.

The shape of the vesicle can influence the overall shape of the clasts (Fisher and Schmincke, 1984). The CIOB pumices have two kinds of vesicles: i) tabular to sub-parallel with a fibrous appearance, and ii) spherical to sub-spherical. It is observed that 60% of the CIOB pumices have elongated vesicles the rest being either spherical (30%) or fibrous (10%) or a combination of both types of vesicles. Distortion and stretching of vesicles occur during vesiculation, extrusion and flowage (Fig. 8 a), although the smaller vesicles tend to be spherical. Pumices with spherical vesicles suggest conditions of high vapor pressure during eruption, where as fibrous pumices are typical of low pressure eruption (Ewart, 1963). According to Kato (1987), a very fibrous variety of pumice called as woody pumice is generated by a cycle where water intrusion leads to progressive quenching, leading to an increase in cracks and the permeability of pore which further results in enhanced water intrusion and sinks the pumice much faster.

Cashman and Fiske (1991) reported that the vesicles in pumice erupted below sea level, and remaining below sea level, will not contain any air but will be inflated only with the hot magmatic gases. As the pumice quenches in the surrounding seawater, these trapped gases cool rapidly and the condensation of the magmatic steam allows pumice to be saturated with seawater and the pumice sinks. Magma fragmentation is also promoted by quench contraction as magma rapidly dissipate its

heat (Morelli and Carey, 2004). The Krakatau eruption is suggested to be sub-aerial and did not involve significant interaction with seawater as evident from the coarse nature of the ignimbrites and presence of tube pumice caused by degassing (Self and Rampino, 1981). But CIOB pumices mostly have elongated (Fig. 8 b) to oval (Fig. 8 d) or spherical vesicles (Fig. 8 c) which may be suggestive of submarine eruption. The study of deepwater explosive eruptions has shown that hydrostatic pressures may be sufficient to suppress magmatic vesiculation. The violence of the eruption will dramatically decrease the production of bubble wall shards and produce a thick, massive sheet composed largely of pumice lapilli that contain highly fibrous vesicles (Busby, 2005).

Izett (1981) presents evidence to show that pumice shards tend to develop from relatively high viscosity rhyolitic magma with temperature  $< 850^{\circ}\text{C}$ , whereas bubble wall and bubble junction shards tend to develop from lower viscosity rhyolitic magma at temperatures  $> 850^{\circ}\text{C}$ . On this premise the CIOB pumice samples with bubble walls and smooth texture (Fig. 6 d) could have resulted from relatively less viscous high temperature magma.

Plagioclase in the CIOB pumices generally has An content of 35-55 while a high value of An 70 is also present. The values are similar to the microprobe data of Mudholkar and Fujii (1995) who suggested that such plagioclases either formed during episodes of magma mixing or from a more mafic magma. This could indicate the possibility of bimodal volcanism during the pumice formation.

Although the details about the origin of pumices recovered from the CIOB are not the main contention of this work but as the source of these pumices is enigmatic, we provide a brief appraisal on this controversial aspect. There are proponents and opponents regarding the in situ or otherwise origin of pumice and glass shards in the CIOB. Venkatarathanam and Biscaye (1973) from a study of zeolites in the CIOB suggested that silicic volcanism might have occurred in the CIOB region. Vallier and Kidd (1977) examined the volcanogenic sediments in the Indian Ocean and opined that abundant silicic volcanic glass was derived during Miocene times. It has been proposed that pumice in the Indian Ocean (Frick and Kent, 1984) and the CIOB (Iyer and Karisiddaiah, 1988; Mukherjee and Iyer 1999; Mudholkar and Fujii, 1995) is largely derived from the 1883 Krakatau eruption and drifted to the present site. Pattan et al. (2008) postulated that the dacitic pumices from the CIOB belong to the 1883 Krakatau eruption while the rhyolitic ones are from the Youngest Toba Tuff eruption of  $\sim 74$  ka from Northern Sumatra. Interestingly, Svalnov (1981) found that the products from Krakatau do not occur in any significant amount in recent sediments that occur to the east of  $80^{\circ}\text{E}$ . The frequent occurrence of pumice to the west of the Ninety East Ridge and the absence of a

favourable surface current circulation patterns in this region (Fairbridge, 1966; Frick and Kent, 1984) cast doubt on the drift theory for the CIOB pumice.

Although pumice recovered from deeper areas of the oceans is thought to be exotic, subaqueous occurrence of pumice has been reported. For instance, in the Atlantic Ocean pumice was reported over submarine volcanoes at depths of 1500 to 2000 m (Neumann von Padang, 1967), near Tonga at depths >1500 m (Fouquet et al., 1991); Okinawa Trough, South of Japan (Halbach et al., 1989) and trachytic pumice flows from intraplate volcanoes in the Society and Austral hotspot regions (depth = 3500 m, Binard et al., 1992). Similar observations were made at depths >1500 m in the Indian Ocean by Hedervari (1982) who suggested an in situ origin from an inferred submarine volcano near the central part of the Ninety East Ridge. Studies by Iyer and Sudhakar (1993, 1995) led to the postulation of a possible in situ submarine silicic volcanism as a source of pumice in the CIOB. Collectively these discoveries strongly suggest that widely distributed pumiceous fragments have recently erupted at great depths from submarine volcanoes.

Iyer and Sudhakar (1993) noted that on a regional scale, structural features seem to control the disposition of manganese nodule deposits in the CIOB. The trends of seamounts and the near north-south orientation of the fracture zones (Das et al., 2007) correlate with the distribution of ore grade manganese nodules. It is note worthy that these deposits occur within and in the vicinity of the pumice field. Nodules with pumice nucleus are are maily distributed along both sides of 76.5° and 79° E fracture zone between 10.5° and 14.5°S (Vineesh et al.2009). Juxtaposition of both these fields and observations based on nodule nuclei (Sarkar et al., 2008) suggest the role of pumice on the occurrence of manganese nodules in the basin. Such a relationship exists in the Clarion-Clipperton Zone, Pacific Ocean, where the abundance of pumices as nuclei seems to have influenced the distribution of nodules (von Stackelberg, 1987). In the CIOB, so far, there are no reports of occurrence of pumice north of 10° S, which corroborate with a paucity of nodules.

Similar to the divisive view about the origin of the pumices, that of glass shards in the CIOB is also thought provoking. The super eruption of Toba volcano ~74 ka ago in northern Sumatra (Rose and Chesner, 1987) resulted in widespread fallout of tephra that covered more than 3000 km in a northwesterly direction. Although Pattan et al. (1999) ascribed the glass shards recovered from sediment cores in the CIOB to the Younger Toba Tuff but Sukumaran et al. (1999) contested this observation. Based on  $^{230}\text{Th}_{\text{xs}}$  values and radiolarian stratigraphy, those authors favoured an in situ deposition of the shards consequent to suboceanic volcanic activities during periods of elevated glaciation. The morphology and composition of the shards have also provided proof of intra-plate

volcanism as a source for these shards (Iyer et al., 1997; Mascarenhas-Pereira et al., 2006). Therefore the sources of pumices and the glass shards that occur in the CIOB are yet to be satisfactorily resolved and this would help open many exciting research avenues.

## **6. Conclusions**

A study of about 400 pumice clasts from the CIOB shows that 32% of the clasts are oblate, 31% are equant and 21% are prolate in shape. The morphology of the clasts affects the settling velocities hence the settling velocities are expected to be close to that of a sphere for the equant clasts that could remain in suspension for a longer time as compared to the non-equant clasts. The non-equant clasts that are oblate or prolate must have settled rapidly. Therefore, the source for non-equant clasts is perhaps near the site of deposition, while the equant clasts may have drifted from a distant source.

Several of the CIOB pumices are seen to have bubble wall and triple junctions that are a result of formation under high temperatures ( $>850^{\circ}$  C) from a less viscous rhyolitic magma. The presence of oblate and elongated bubbles and vesicles also indicate higher-pressure conditions than that required for tube vesicles.

The physical properties density, specific gravity, void ratio, degree of saturation and porosity are interrelated and along with the shape of the clasts determine the settling of the pumice. The other factors influencing the settling velocities are accumulation of suspended sediments into the vesicles and habitation of organisms on the clasts.

## **7. Acknowledgements**

We thank the Director for permission to publish this paper. We acknowledge the help received from V. Khedekar (SEM-EDS), B. Vijay Kumar (access to sample repository) and S. Jai Sankar (sample locations). NK is thankful for the financial assistance provided under the CSIR (New Delhi) Fellowship scheme. This is NIO's contribution # ???. We deeply acknowledge the reviewers for the suggestions that helped to improve the manuscript and Dr. Jiang Shaoqing for encouragement to revise the manuscript.

## References

Binard, N., Hekinian, R., Cheminee, J. L. and Stoffers, P., 1992. Styles of Eruptive activity on intraplate volcanoes in the Society and Austral hot spot regions: bathymetry, petrology, and submersible observations. *J. Geophys. Res.*, 97: 13999-14015.

Binns, R. E., 1972. Composition and derivation of pumice on postglacial strandlines in northern Europe and the western Arctic. *Geol. Soc. Amer. Bull.*, 83: 2303–2324.

Bryan, W. B., 1971. Coral Sea drift pumice stranded on Eua Island, Tonga, in 1969. *Geol. Soc. Amer. Bull.*, 82: 2799-2812.

Busby, C., 2005. Possible distinguishing characteristics of very deepwater explosive and effusive silicic volcanism. *Geology*, 33: 845-848.

Cashman K. V. and Fiske R. S., 1991. Fallout of pyroclastic debris from submarine volcanic eruptions. *Science*, 253: 241-352.

Das, P., Iyer S. D. and Kodagali V. N., 2007. Morphological characteristics and emplacement mechanism of the seamounts in the Central Indian Ocean Basin. *Tectonophysics*, 443: 1-18.

Esposito, L. and Guadagno, F. M., 1998. Some special geotechnical properties of pumice deposits. *Bull. Eng. Geol. Env.*, 57: 41–50.

Ewart, A., 1963. Petrology and petrogenesis of the Quaternary pumice ash in the Taupo area, New Zealand. *J. Petrol.*, 4: 392-431.

Fairbridge, R. W., 1966. *The encyclopedia of oceanography*, Reinhold, New York, 1021.

Fisher, R. V. and Schmincke H. U., 1984. *Pyroclastic rocks*. Springer-Verlag, Berlin, 472 .

Fouquet, Y., von Stackelberg, U., Charlou, J. L., Donval, J. P., Eringer, J., Foucher, J. P., Herzig, P., Muhe, R., Soakai, S., Wiedicke, M. and Whitechurch, H., 1991. Hydrothermal activity and metallogenesis in the Lau back-arc basin. *Nature*, 349: 778-781.

Frick, C. and Kent, L. E., 1984. Drift pumice from the Indian and South African Oceans. *Trans. Geol. Soc. S. Afr.*, 87: 19–33.

Gardner, J. E., Thomas, R. M. E., Jaupart C. and Tait, S., 1996. Fragmentation of magma during Plinian volcanic eruptions. *Bull Volcanol.*, 58: 144–162.

Goldbery, R. and Richardson, D., 1989. The influence of bulk shape factors on settling velocities of natural sand-sized sedimentary suites. *Sediment.*, 36: 125-136.

Halbach, P., Sattler, C., Teichmann, R. and Otten, P., 1989. Cobalt rich and platinum bearing manganese crust deposits on seamounts: Nature, formation metal potential. *Mar. Min.*, 8: 23-39.

Hedervari, P., 1982. A possible submarine volcano near the central part of Ninetyeast ridge, Indian Ocean. *J. Volcanol. Geotherm. Res.*, 13: 199-211.

Heiken, G. and Eichelberger, J., 1980. Eruptions at Chaos Crags, Lassen Volcanic National Park, California. *J. Volcanol. Geotherm. Res.*, 7: 443-481.

Iyer, S. D., 2005. Pumice from the Central Indian Ocean Basin. *National seminar on polymetallic nodules*. Regional Research Laboratory, Bhubaneswar, 29-30<sup>th</sup> September 2005.

Iyer, S. D. and Karisiddaiah, S. M., 1988. Morphology and petrography of pumice from the Central Indian Ocean Basin. *Indian J. Mar. Sci.*, 17: 333-334.

Iyer, S. D. and Sudhakar, M., 1993. Coexistence of pumice and manganese nodule fields: evidence for submarine silicic volcanism in the Central Indian Basin. *Deep-Sea Res.*, 40: 1123-1128.

Iyer, S. D. and Sudhakar, M., 1995. Evidences for a volcanic province in the Central Indian Basin. *J. Geol. Soc. Ind.*, 46: 353-358.

Iyer, S. D., Shyam Prasad, M., Gupta, S. M. and Charan S. N., 1997. Evidence for recent hydrothermal activity in the Central Indian Basin. *Deep-Sea Res. I*, 44 :1167-1184.

Izett, G. A., 1981. Volcanic ash beds: Recorders of Upper Cenozoic silicic pyroclastic volcanism in the Western United States. *J. Geophys. Res.*, 86: 10200-10222.

Jimenez, J. and Madsen, O., 2003. A simple formula to estimate settling velocity of natural sediments. *J. Waterway Port Coast Ocean Eng.*, 129: 70-78.

Kalangutkar, N. G., Iyer S. D. and Matta V. M., 2007. A report on findings of pumices from the Central Indian Ocean Basin. *IUGG 2007 Perugia Italy - XXIV IUGG General Assembly*. pp 29.

Kato, Y., 1987. Woody pumice generated with submarine eruption. *J. Geol. Society Japan*, 93: 11-20.

Klug, C., Cashman, K.V. and Bacon, C. R., 2002. Structure and physical characteristics of pumice from the climactic eruption of Mt. Mazama (Crater Lake), Oregon. *Bull. Volcanol.*, 64: 486-501.

Kodagali, V. N., 1998. A pair of seamount chains in the Central Indian Basin identified from multibeam mapping. *Mar. Geol.*, 21: 147-158.

Komar, D. and Reimers, C. E., 1978. Grain shape effects on settling rates. *J. Geol.*, 86: 193-209.

Mangan, M.T. and Cashman, K.V., 1996. The structure of basaltic scoria and reticulite and inferences for vesiculation, foam formation, and fragmentation in lava fountains. *J. Volcanol. Geotherm. Res.* 73: 1-18.

Manville, V., White, J. D. L., Houghton, B. F. and Wilson, C. J. N., 1998. The saturation behaviour of pumice and some sedimentological implications. *Sed. Geol.* 119: 5-16.

Martin-Barajas, A., Lallier-Vergas, E., (1993). Ash layers and pumice in the Central Indian Basin: relationship to the formation of manganese nodules. *Mar. Geol.*, 115: 307-329.

Mascarenhas-Pereira, M. B. L., Nath, B. N., Borole, D. V. and Gupta, S. M., 2006. Nature, source and composition of volcanic ash in sediments from a fracture zone trace of Rodriguez Triple Junction in the Central Indian Basin. *Mar. Geol.*, 229: 79-90.

Morelli, D. and Carey, S., 2004. Morphology of pumice from different pyroclastic transport regimes. *IAVCEI General assembly Pucon Chile*, 15<sup>th</sup> Nov 2004. 3-a, *Explosive Volcanism*. Poster Session Programme.

Mudholkar, A. and Fujii, T., 1995. Fresh pumice from the Central Indian Basin: a Krakatau 1883 signature. *Mar. Geol.*, 125: 143-151.

Mukherjee, A. D. and Iyer, S. D., 1999. Synthesis of morphotectonics and volcanics of the Central Indian Ocean Basin. *Curr. Sci.*, 76: 296-304.

Mukhopadhyay, R., Iyer, S.D. and Ghosh, A.K., 2002. The Indian Ocean nodule field: petrotectonic evolution and ferromanganese deposits. *Earth-Science Rev.*, 60: 67-130.

Neumann von Padang, M., 1967. Catalogue of active volcanoes of the world. Part XXI Atlantic Ocean. *Inter. Volcanol. Asso.. Napoli*. pp. 128.

Nishimura, S., Harjono, H., and Suparka, S., The Krakatau islands: The geotectonic setting. *GeoJournal*. 1992, 28: 87-98.

Pattan, J. N., Mudholkar, A. V., Jai Sankar, S. and Ilangoan, D., 2008. Drift pumice in the Central Indian Ocean Basin: geochemical evidence. *Deep-Sea Res. I*, 55: 369–378.

Pattan, J. N., Shane, P. and Banakar, V. K., 1999. New occurrence of Youngest Toba Tuff in abyssal sediments of the Central Indian Ocean. *Mar. Geol.*, 155: 243-248.

Polacci, M., Papale, P. and Rosi, M., 2001. Textural heterogeneities in pumices from the climactic eruption of Mt. Pinatubo, 15 June 1991, and implications for magma ascent dynamics, *Bull. Volcanol.*, 63: 83-97.

Polacci, M., Pioli, L. and Rosi, M., 2003. The Plinian phase of the Campanian ignimbrite eruption (Phlegrean Fields, Italy): evidence from density measurements and textural characterization of pumice. *Bull. Volcanol.*, 65: 418-432.

Risso, C., Scasso, R. A. and Alfredo A., 2002. Presence of large pumice blocks on Tierra del Fuego and South Shetland Islands shorelines, from 1962 South Sandwich Islands eruption. *Mar. Geol.*, 186: 413-422.

Rose, W. I. and Chesner, C. A., 1987. Dispersal of ash in the great Toba eruption, 75 ka. *Geology*, 15: 913–917.

Sarkar C., Iyer S. D. and Hazra S., 2008. Inter-relationship between nuclei and gross characteristics of manganese nodules, Central Indian Ocean Basin. *Mar. Geores. Geotech.*, 26: 259-289.

Self, S. and Rampino, M. R., 1981. The 1883 eruption of Krakatau. *Nature*, 294: 699-704.

Sparks, R. S. J., 1978. The dynamics of bubble formation and growth in magmas: a review and analysis. *J. Volcanol. Geotherm. Res.*, 3: 1-37.

Sudhakar, M., Iyer, S. D. and Mislankar, P. G., 1992. Does pumice control the characteristics and distribution of ferromanganese nodules in Central Indian Basin?. *Abst. 29th Intern. Geol. Cong.*, Kyoto, Japan, Aug. 24 - Sep. 3.



Sukumaran, N. P., Banerjee, R., Borole, D. V. Gupta, S. M., 1999. Some aspects of volcanic ash layers in the Central Indian Basin. *Geo-Mar. Lett.*, 18: 203-298.

Svalnov V. N., 1981. The effect of island volcanism in the Indian Ocean. *Oceanology*, 21: 606-612.

Vallier, T. L. and Kidd, R. B., 1977. Volcanogenic sediments in the Indian Ocean. In J.R. Heirtzler et al. (Eds.), *Indian Ocean Geology and Biostratigraphy studies following DSD legs 22-29, Am. Geophy. Union*, pp. 87-118. Washington, D. C.

Venkatarathnam, K. and Biscaye, P.E., 1973. Deep sea zeolites: Variations in space and time in the sediments of the Indian Ocean. *Mar. Geol.*, 15: M11-M17.

Vineesh, T.C., Nath, B. N., Banerjee, R., Jaisankar, S. and Lekshmi, V., 2009. Manganese nodule morphology as indicators for oceanic processes in the Central Indian Basin. *Inter. Geol. Rev.* 51: 27-44.

von Stackelberg U., 1987. Pumice and buried manganese nodules from the equatorial North Pacific Ocean. *Geol. Jahrbuch*. D87. 229-285.

Whitham, A. G. and Sparks R. S. J., 1986. Pumice. *Bull. Volcanol.*, 48: 209-223.

Wilson, L. and Huang, T. C., 1979. The influence of shape on the atmospheric settling velocity of volcanic ash particles. *Earth Planet. Sci. Lett.*, 44: 311-324.

Zhang, Y., 1998. Experimental simulation on gas-driven eruption: kinetics of bubble growth and effect of geometry. *Bull. Volcanol.*, 59: 281-290.

Zingg, Th., 1935. Beitrag zur Schotteranalyse. Schweiz. *Min. Petr. Mitt.*, 15: 39-140.

## CAPTIONS TO FIGURES

**Fig. 1:** Station location map for the pumices studied of the CIOB. Red solid circles = Sample locations, FZ = Fracture Zones, Stars = Seamounts, A to H seamount chains along propagative fracture zones. IOTJ=Indian Ocean Triple Junction. Contour intervals are in 100 m. Base map after Das et al. (2007).

**Fig. 2 (a):** Zingg's diagram illustrating the distribution of shape of 400 pumices into different quadrants. **(b):** Histogram of Corey's shape factor (CSF) versus the frequency of occurrence of samples of each class.

**Fig. 3:** Plots of the measured dimensions of the CIOB pumices. (a) c/b and (b) c/a plots show a linear trend with CSF while (c) b/a does not show a good correlation with CSF.

**Fig. 4:** Pumice samples of variable shapes and sizes, some of which have ferromanganese oxide coating.

**Fig. 5:** Plot of sinking time vs density. The samples show increases in density due to different degrees of saturation with increasing time. It was seen that the pumice cubes sank once their sinking weight approximately equaled their volume, i.e when the density nears unity. 1-30 = samples studied

**Fig. 6:** Binocular microscopy (a) elongated vesicles showing swirled glassy texture, (b) oval bubbles near a feldspar grain, (c) augite crystal in vesicle. (d) Smooth textured pumice. Photomicrographs (cross-polarized light), (e) plagioclase grains showing zoning (x25) (f) glomeroporphyritic texture exhibited by lamellar plagioclase laths and pyroxenes (x25)

**Fig.7:** X-ray diffraction of pumices. Note that glass hump between 20 ° and 30 °. Q= Quartz, P = Plagioclase, QC = Quartz-Cristobalite.

**Fig.8:** Electron micrographs showing (a) swirled glass and vesicles, (b) tube vesicles, (c) spherical vesicles, (d) oval vesicles with bubble wall triple junction, (e) change in vesicle shape, (f) crystal with glass coating. (g) radiolarians in vesicles, (h) botryoidal FeMn coating on pumice.

## CAPTION TO TABLE

**Table 1:** Physical properties and nature of the CIOB pumices. nd = not determinable due to less quantity of sample.

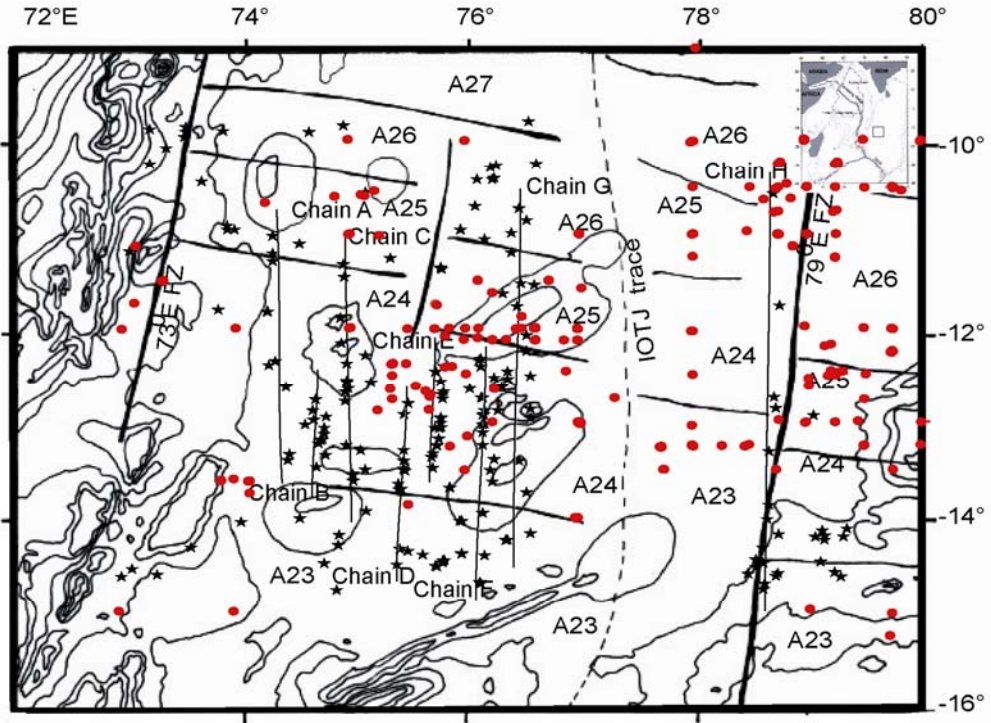


Fig.1

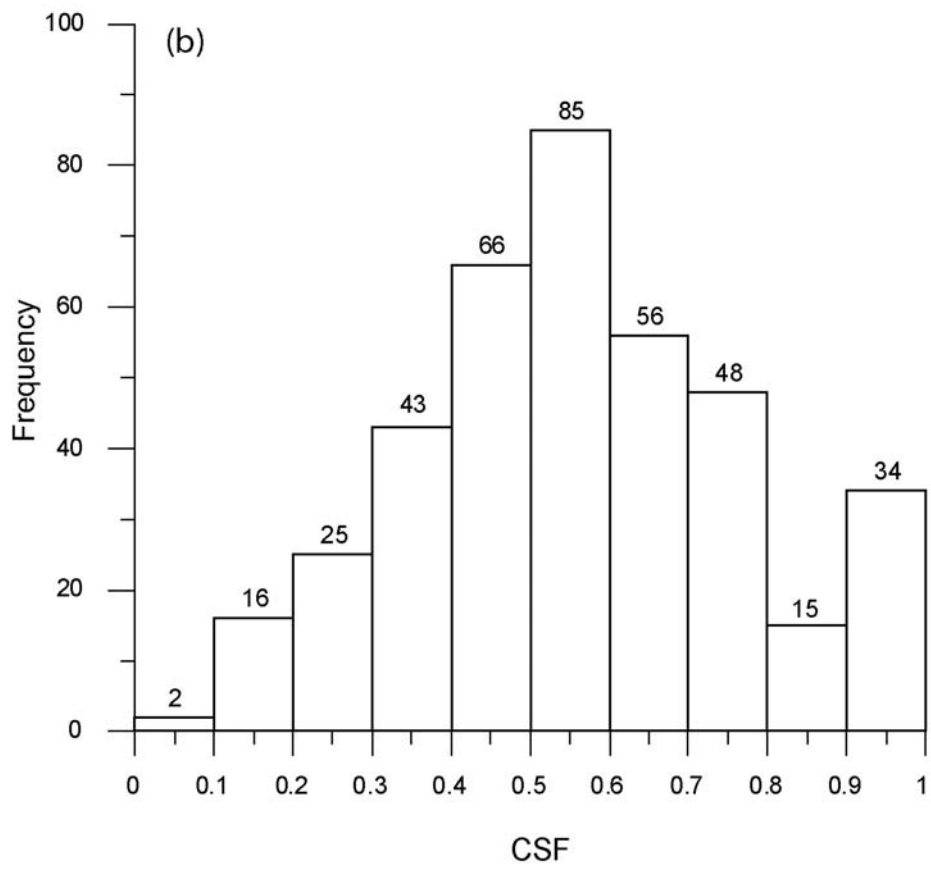
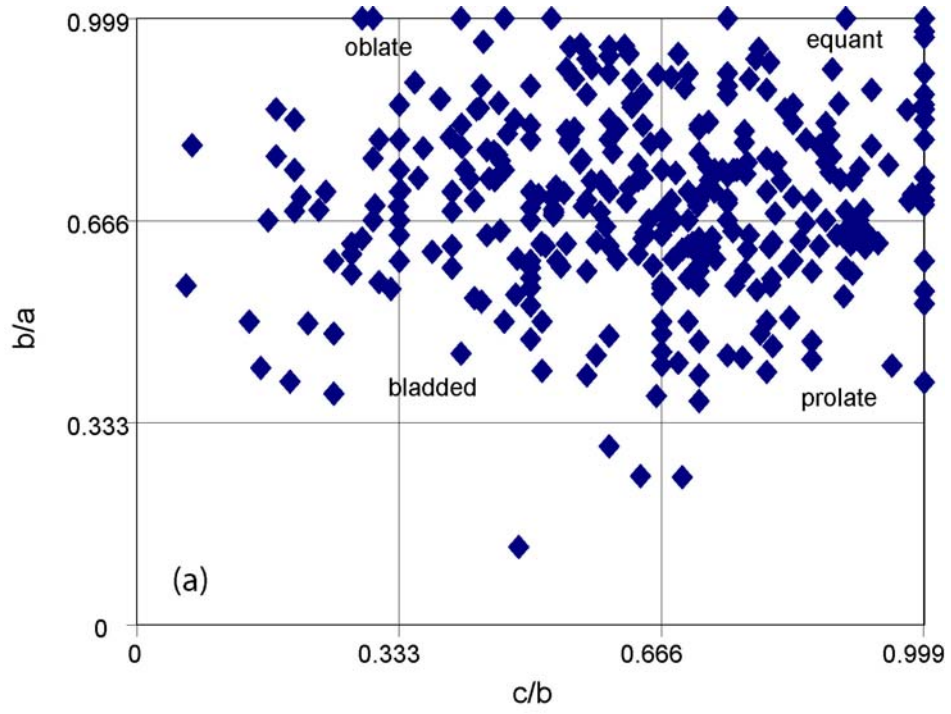


Fig. 2

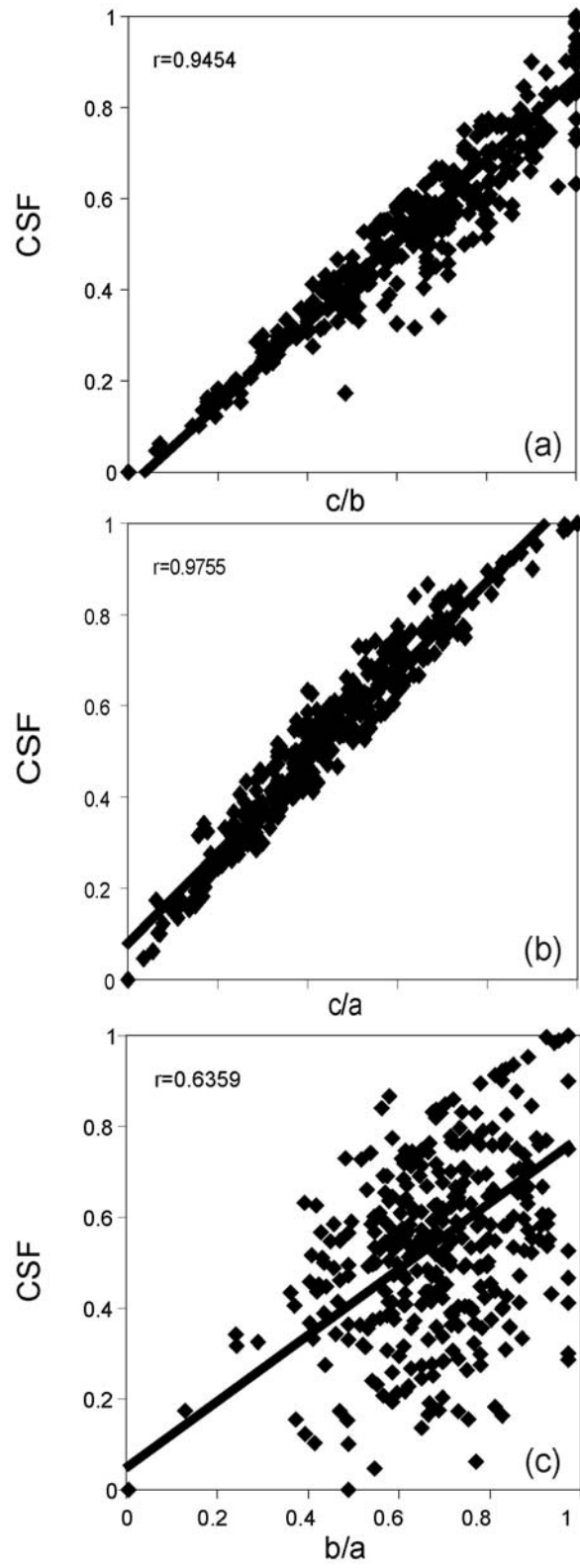


Fig. 3



Fig. 4

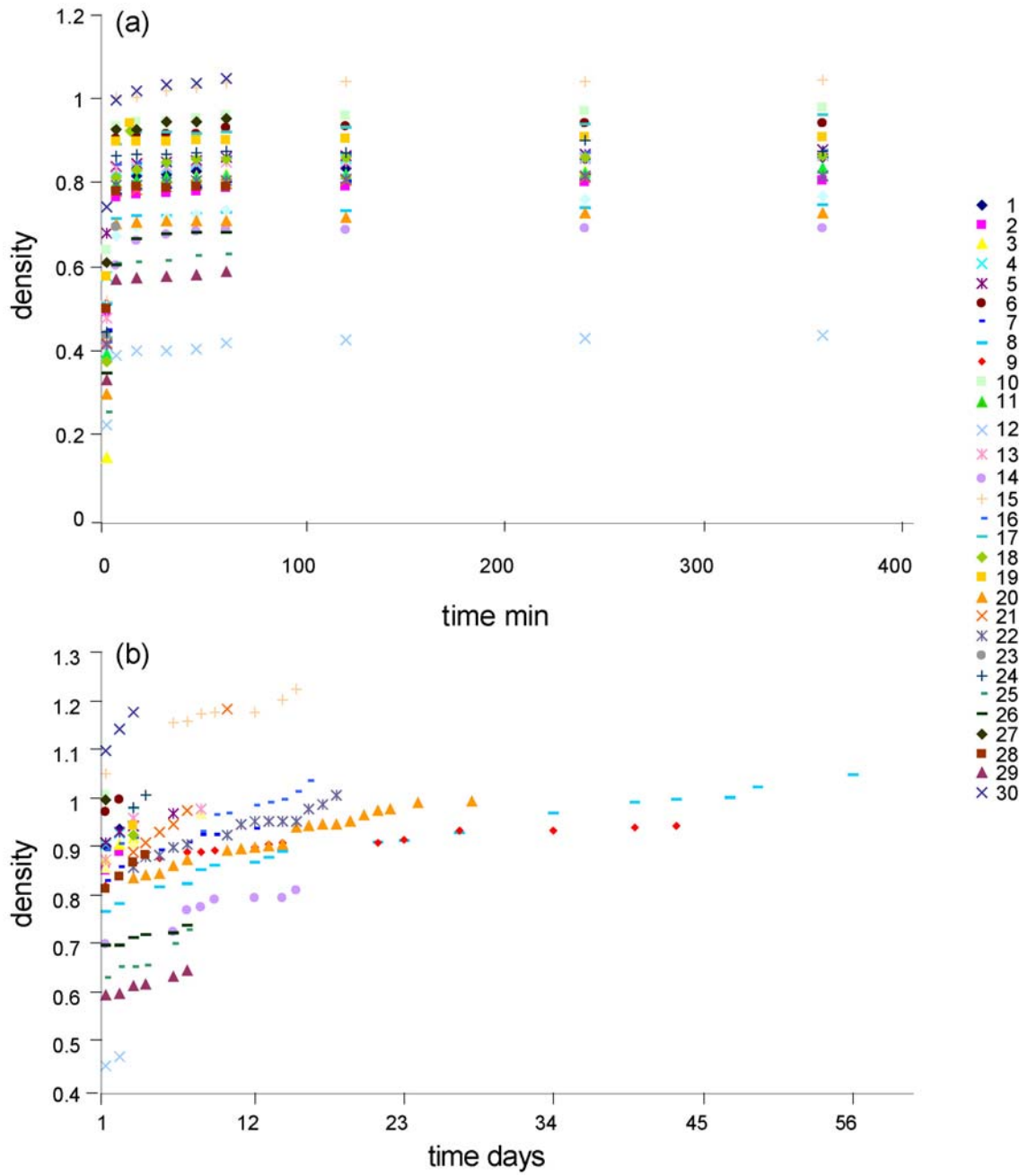


Fig. 5

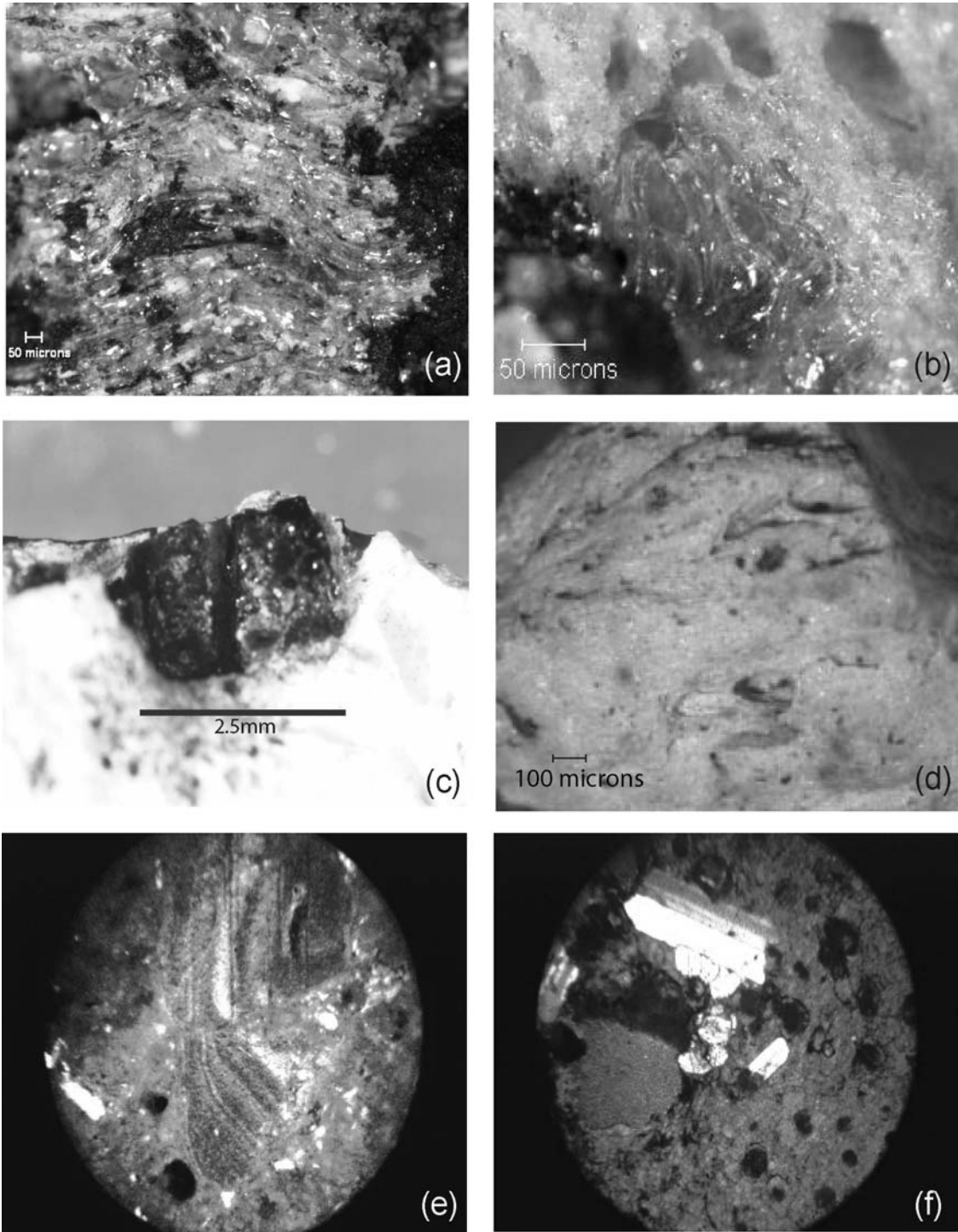


Fig. 6



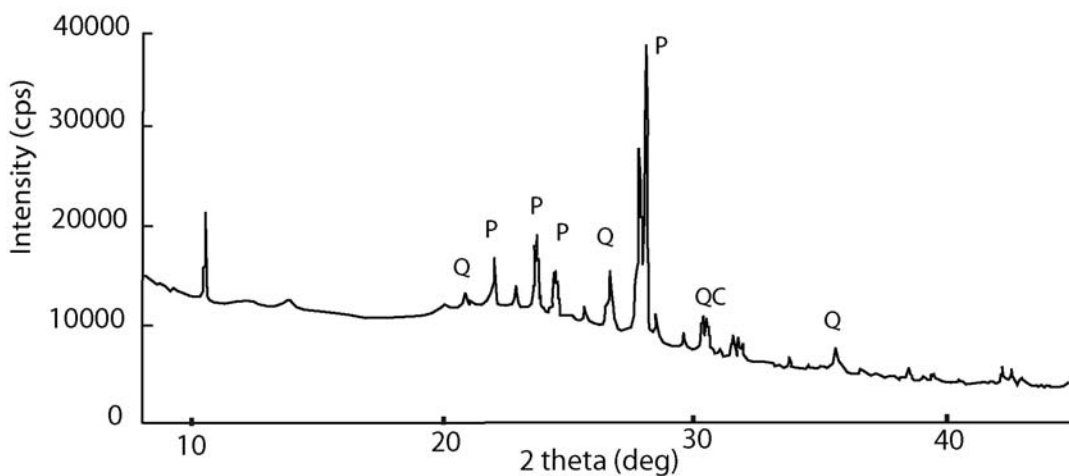
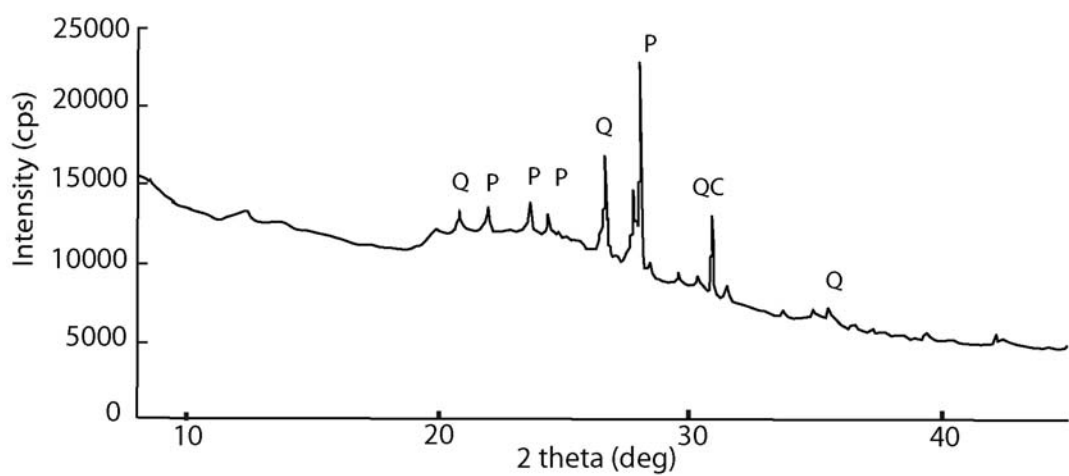


Fig. 7

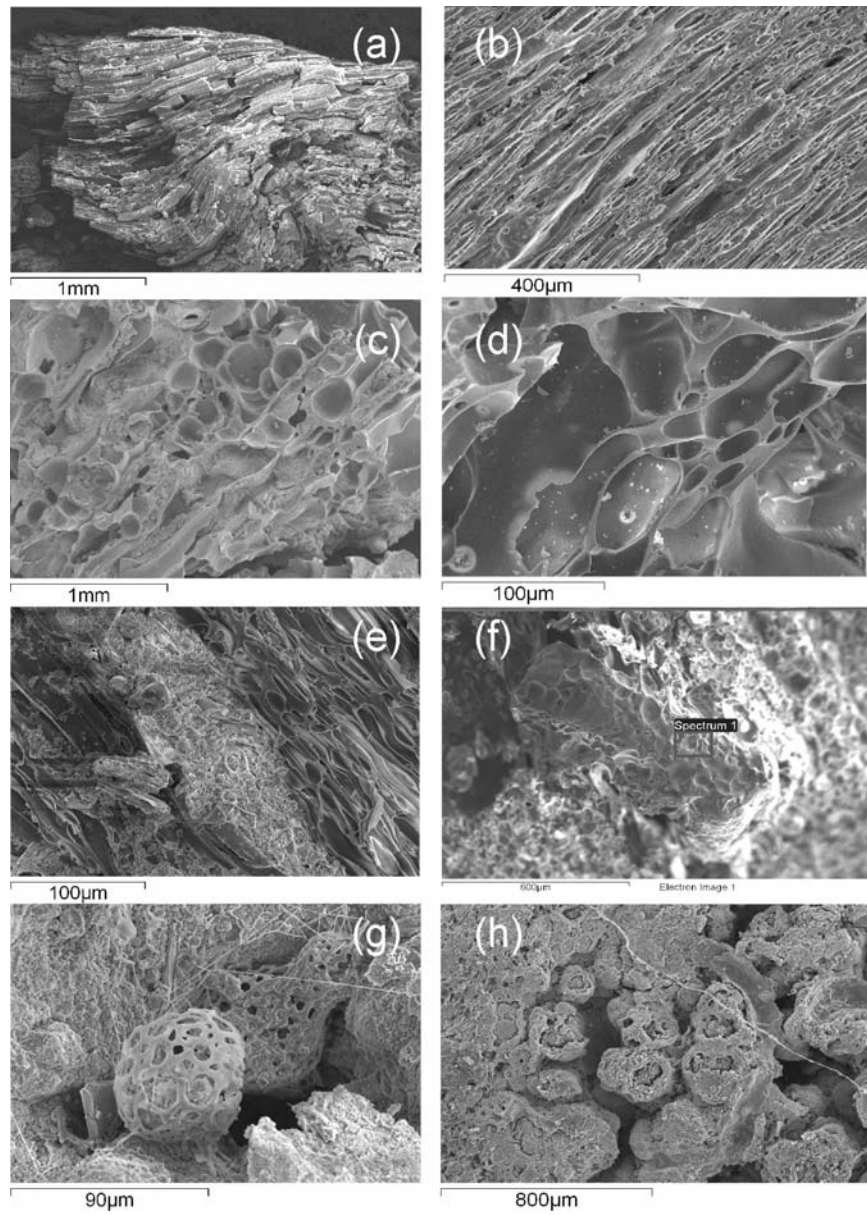


Fig. 8

Table 1

	Station No	Dry weight	Weight at sinking	Dry Density	Specific gravity	Void ratio	Moisture content during sinking	Degree of saturation	Saturation density	Porosity	Nature of pumice and vesicles	Sinking time
		(gm)	(gm)	(gm/cc)	(G)	(e)		(S%)	(gm/cc)	(%)		(days)
1	SS12/676KK	0.76	1.41	0.50	2.18	3.48	0.85	53.50	1.31	77.66	Non- coated, fibrous vesicles	<2
2	AAS 3/B15/62	1.36	2.53	0.49	2.48	4.20	0.86	50.50	1.33	80.77	Non- coated, elongated fibrous	<2
3	F380	0.97	1.59	0.56	2.54	3.66	0.64	44.49	1.38	78.53	Non- coated, elongated fibrous	<2
4	NRI27	2.06	2.97	0.67	2.48	2.83	0.44	38.94	1.43	73.90	Non- coated, elongated	<2
5	SS6/372	0.83	1.66	0.50	2.37	3.94	1.00	60.30	1.32	79.74	Non- coated, elongated	<2
6	AAS 3/B15/59	1.02	2.01	0.51	3.27	5.61	0.97	56.21	1.39	84.88	Non- coated, elongated	>2
7	SS13/681A	1.39	2.98	0.44	2.51	4.95	1.15	58.07	1.30	83.20	FeMn oxides in vesicle, elongated oval	>2
8	AAS 3/ B15/67	0.66	1.38	0.50	2.75	4.71	1.10	64.00	1.35	82.49	FeMn oxide in vesicles, spherical	>2
9	SS12/676D	2.39	5.73	0.39	2.69	6.11	1.40	61.77	1.28	85.93	Non- coated, fibrous	>2
10	F1/41B	2.30	3.63	0.64	2.47	3.01	0.58	47.52	1.41	75.05	FeMn oxide in vesicles, oval	>2
11	NR2/86E	0.86	2.17	0.38	2.41	5.56	1.54	66.82	1.26	84.75	Oxide film, spherical	<2
12	SS12/676V	0.39	0.85	0.21	2.41	10.67	1.18	26.58	1.16	91.43	FeMn oxides in vesicles, spherical	>2
13	SKA016 0798E	0.62	1.39	0.43	2.45	4.84	1.25	63.19	1.29	82.88	FeMn oxides in vesicles, elongated	<2

14	AAS3/B15/67	0.61	1.32	0.41	2.53	5.38	1.16	52.83	1.27	84.32	Non- coated, lineated	>2
15	AAS3/B15/67	1.12	2.64	0.52	2.39	3.78	1.36	86.23	1.34	79.08	FeMn oxide in vesicles, spherical vesicles	>2
16	NR 2/ 86 E	0.58	1.32	0.43	2.54	4.92	1.29	66.42	1.26	83.10	Non-coated, elongated	<2
17	AAS3/B15/65	1.51	3.75	0.42	2.45	5.10	1.49	73.85	1.29	83.61	FeMn oxide in vesicles, oval elongated	>2
18	AAS3/B15/57	1.35	3.33	0.37	2.37	5.34	1.47	65.31	1.22	84.22	Off white, FeMn Oxide in vesicles, asbestosy	<2
19	AAS26#46	5.84	9.59	0.57	1.84	2.21	0.64	53.51	1.26	68.84	FeMn oxide in vesicles, spherical+ elongated	<2
20	AAS27#12	1.43	4.80	0.30	2.37	7.02	2.35	79.22	1.17	87.53	White, non-coated, Elongated	>2
21	AAS26#33	1.36	3.17	0.42	2.37	4.67	1.32	67.31	1.24	82.36	White, non-coated, Elongated	>2
22	AAS22#16	1.57	3.80	0.41	2.23	4.40	1.43	72.50	1.23	81.47	Non- coated, grey, elongated	>2
23	AAS22#7	1.17	1.91	0.43	2.48	4.72	0.64	33.77	1.26	82.52	Dark grey non- coated spherical	<2
24	AAS3/B15/56	1.13	2.56	0.44	2.55	4.74	1.26	67.97	1.27	82.58	White, non-coated, elongated	>2
25	AAS26#31	1.15	3.33	0.25	2.51	9.08	1.89	52.40	1.15	90.08	Non- coated, elongated fibrous	>2
26	AAS26#16	1.42	3.06	0.34	2.39	5.93	1.15	46.22	1.20	85.58	Non-coated, spherical	>2
27	AAS22#16	2.19	3.41	0.61	nd	nd	0.56	nd	nd	nd	Non- coated, grey, elongated	>2
28	SS13/704C	2.02	3.50	0.50	2.57	4.14	0.74	45.62	1.30	80.55	Non-coated, elongated fibrous	>2
29	SS10/650C	2.26	4.61	0.33	2.39	6.26	1.03	39.41	1.19	86.22	Non- coated, honey comb elongated	>2
30	AAS26#44	2.85	4.38	0.74	2.25	2.03	0.54	59.42	1.41	67.01	Non- coated, fibrous swirling	<2